

# Chemodynamical Properties of Extremely Metal-Poor Stars Observed with Gemini/GRACES

Miji Jeong<sup>1</sup>, Young Sun Lee<sup>2</sup>, Young Kwang Kim<sup>2</sup>, Timothy C. Beers<sup>3</sup>, Vinicius M. Placco<sup>4</sup>

<sup>1</sup>Department of Astronomy, Space Science, and Geology, Chungnam National University, Daejeon 34134, South Korea

<sup>2</sup>Department of Astronomy and Space Science, Chungnam National University, Daejeon 34134, South Korea

<sup>3</sup>Department of Physics and Astronomy, University of Notre Dame, Notre Dame, IN 46556, USA

<sup>4</sup>NSF's NOIRLab, 950 N. Cherry Ave., Tucson, AZ 85719, USA

## Sample Selection & Observations

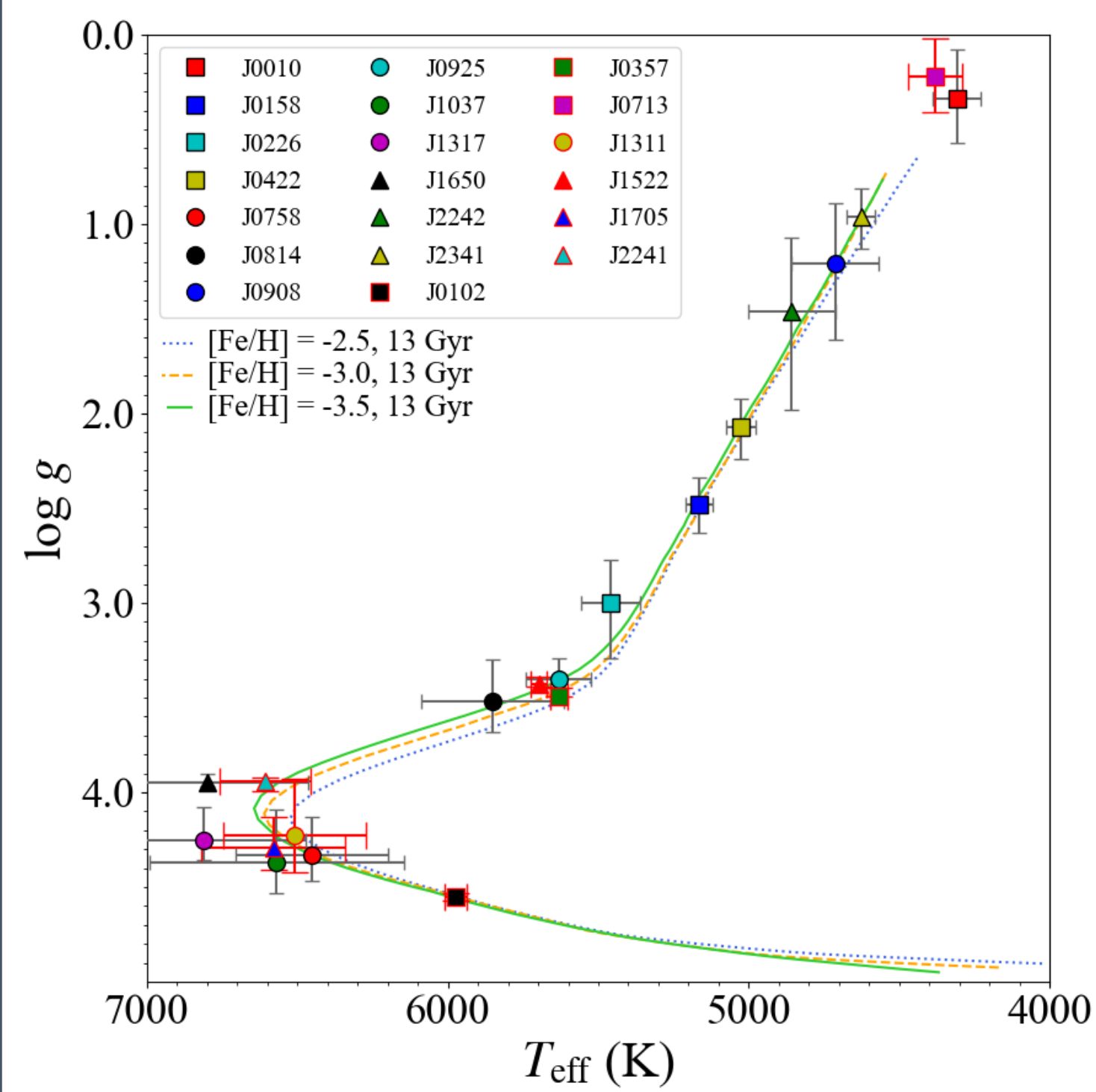
Our program stars were selected from the low-resolution ( $R \sim 2,000$ ) SDSS and LAMOST spectra. We used the metallicity estimate based on the Ca II K in the SEGUE Stellar Parameter Pipeline (SSPP; Lee et al. 2008), which is the sensitivity metallicity indicator for extremely low-metallicity stars.

### Selection Criteria :

- $4000 \text{ K} < T_{\text{eff}} < 7000 \text{ K}$
- $[\text{Fe}/\text{H}] < -2.8$
- $g < 17.0 \text{ mag}$

We obtained high-resolution ( $R \sim 40,000$ ) spectra with GEMINI/GRACES in 2016A, 2018B, and 2019B.

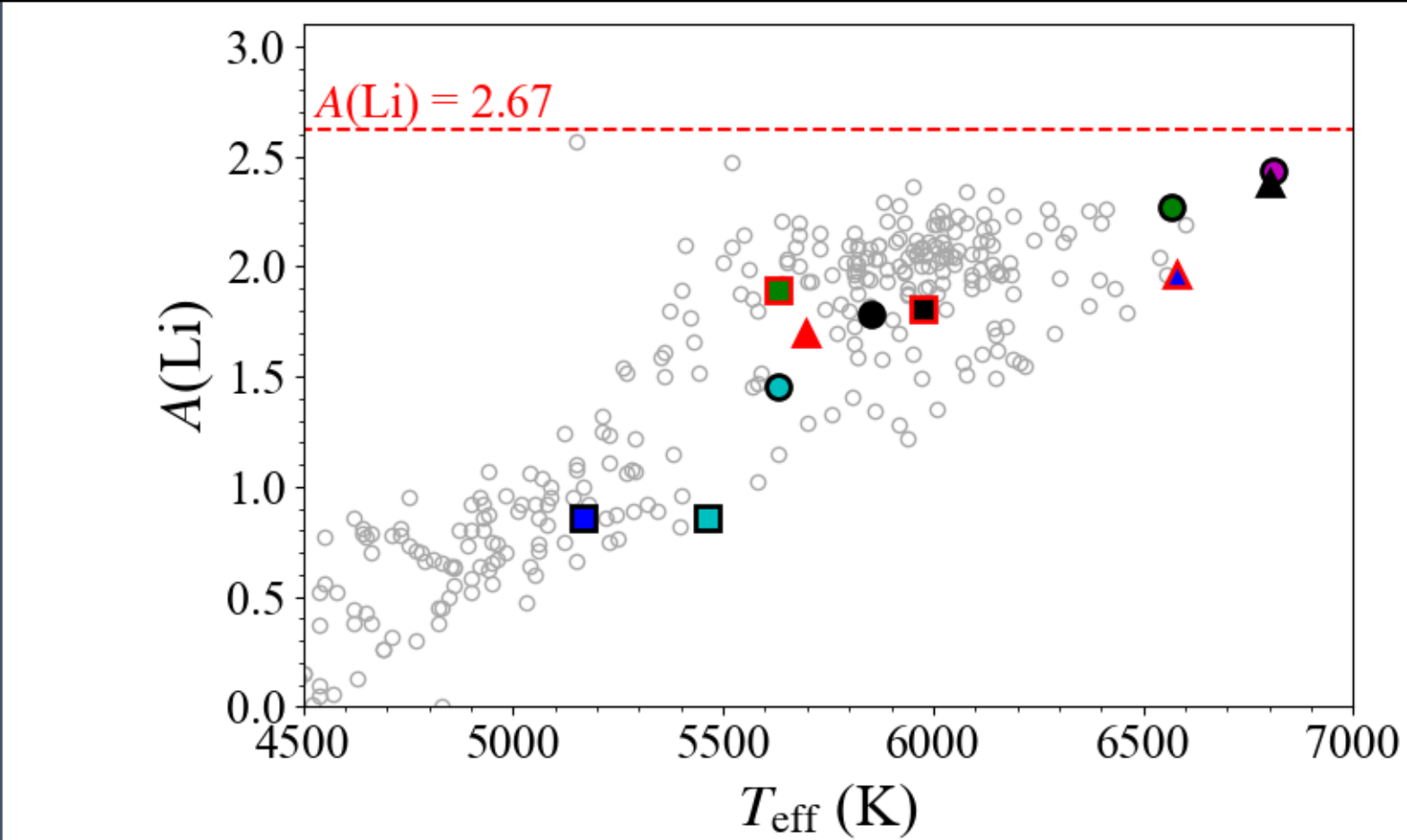
## Derived Stellar Parameters



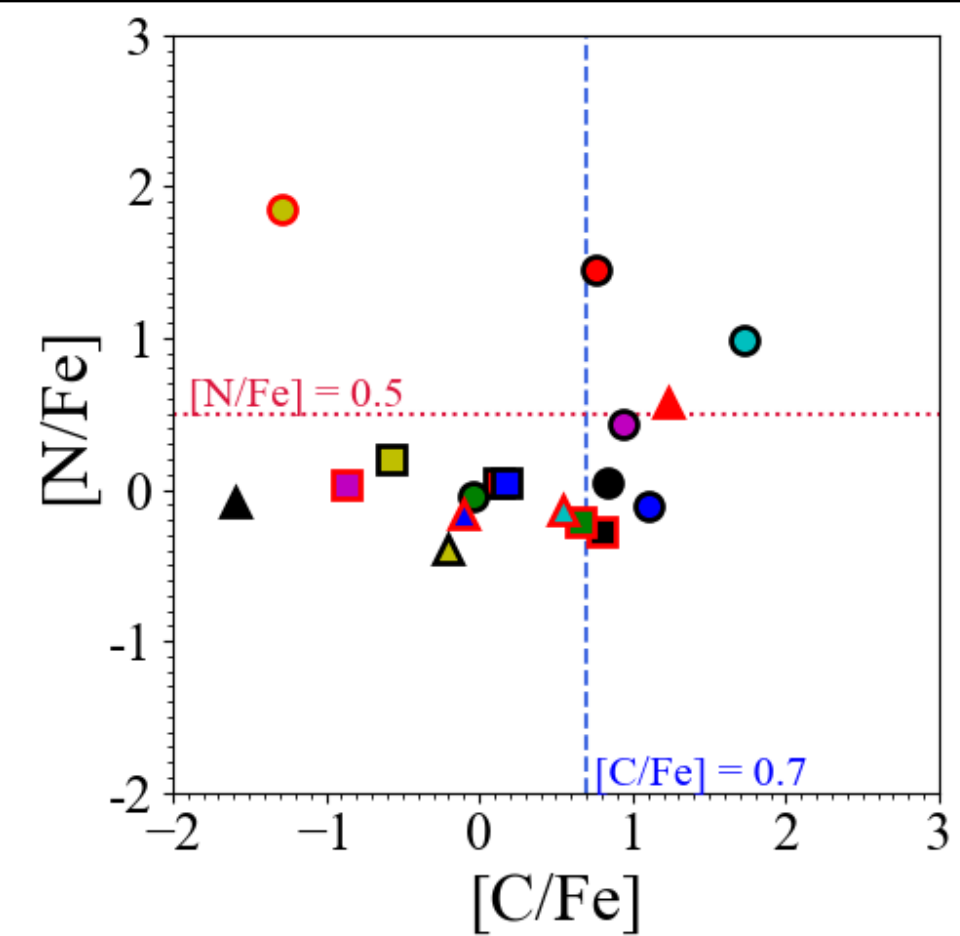
- Our stars are made up of stars at various evolution stages.
- Their metallicity is  $-3.78 \sim -2.17$ , of which 11 are EMP stars, and 9 are VMP stars.
- Stars marked with red edges indicate stars with  $e > 0.7$  in Figure 3.

◀ **Figure 1.** Derived stellar parameters ( $T_{\text{eff}}$ ,  $\log g$ ) of our stars, and overlapped with Yonsei-Yale isochrones with 13 Gyr  $[\alpha/\text{Fe}] = +0.3$  and  $[\text{Fe}/\text{H}] = -2.5$  (green solid),  $-3.0$  (orange dashed),  $-3.5$  (blue dotted).

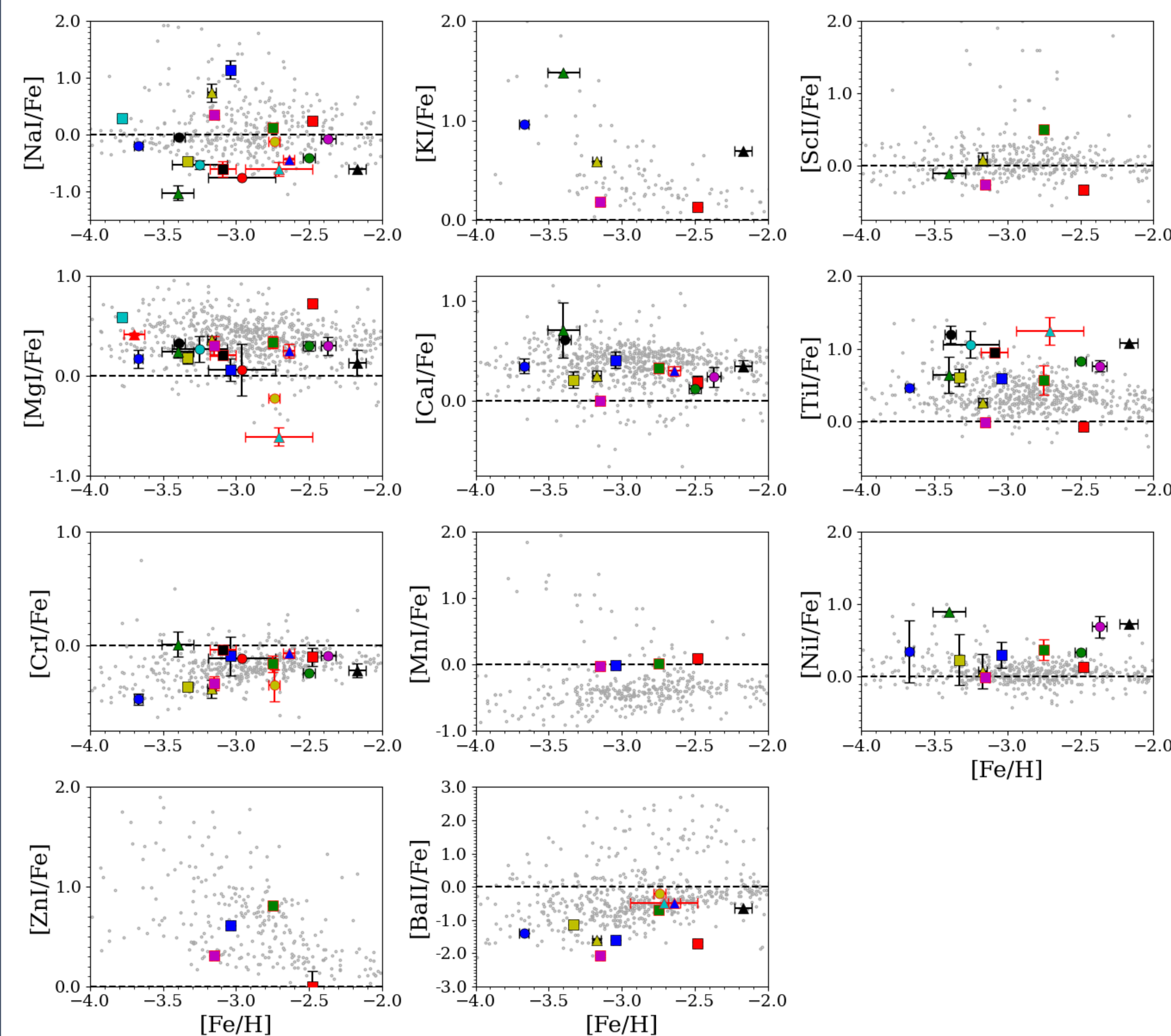
## Results



▲ **Figure 4.** Absolute Li abundances for our program stars, as a function of effective temperature. Grey open circles represent the results of Roederer et al. 2014 and Kielty et al. 2021. Red dashed line Primordial Li predicted by Big Bang nucleosynthesis (Spergel et al. 2007).



▲ **Figure 5.**  $[\text{N}/\text{Fe}] - [\text{C}/\text{Fe}]$  diagram. Blue dashed line indicates  $[\text{C}/\text{Fe}] = +0.7$ , the boundary of CEMP stars. Red dotted line displays  $[\text{N}/\text{Fe}] = +0.50$ .

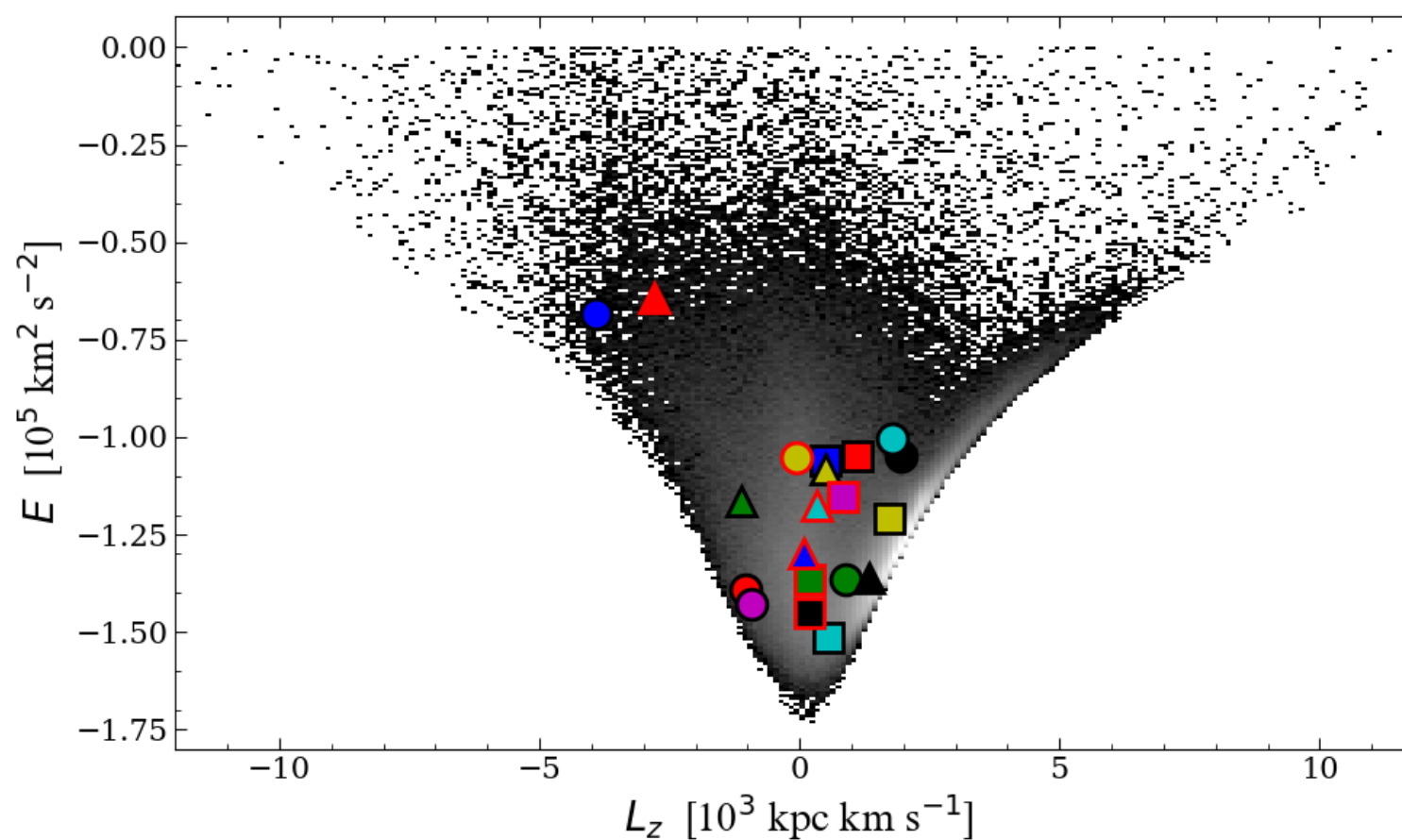


▲ **Figure 6.** Abundance ratios of odd-Z (Na, K, Sc), even-Z (Mg, Ca, Ti), Fe-peak (Cr, Mn, Ni, Zn), and n-capture (Ba) in our program stars and stars in MW halo in comparison with those of other literature stars (Venn et al. 2004, Aoki et al. 2013, Yong et al. 2013, Roederer et al. 2014, Kielty et al. 2021).

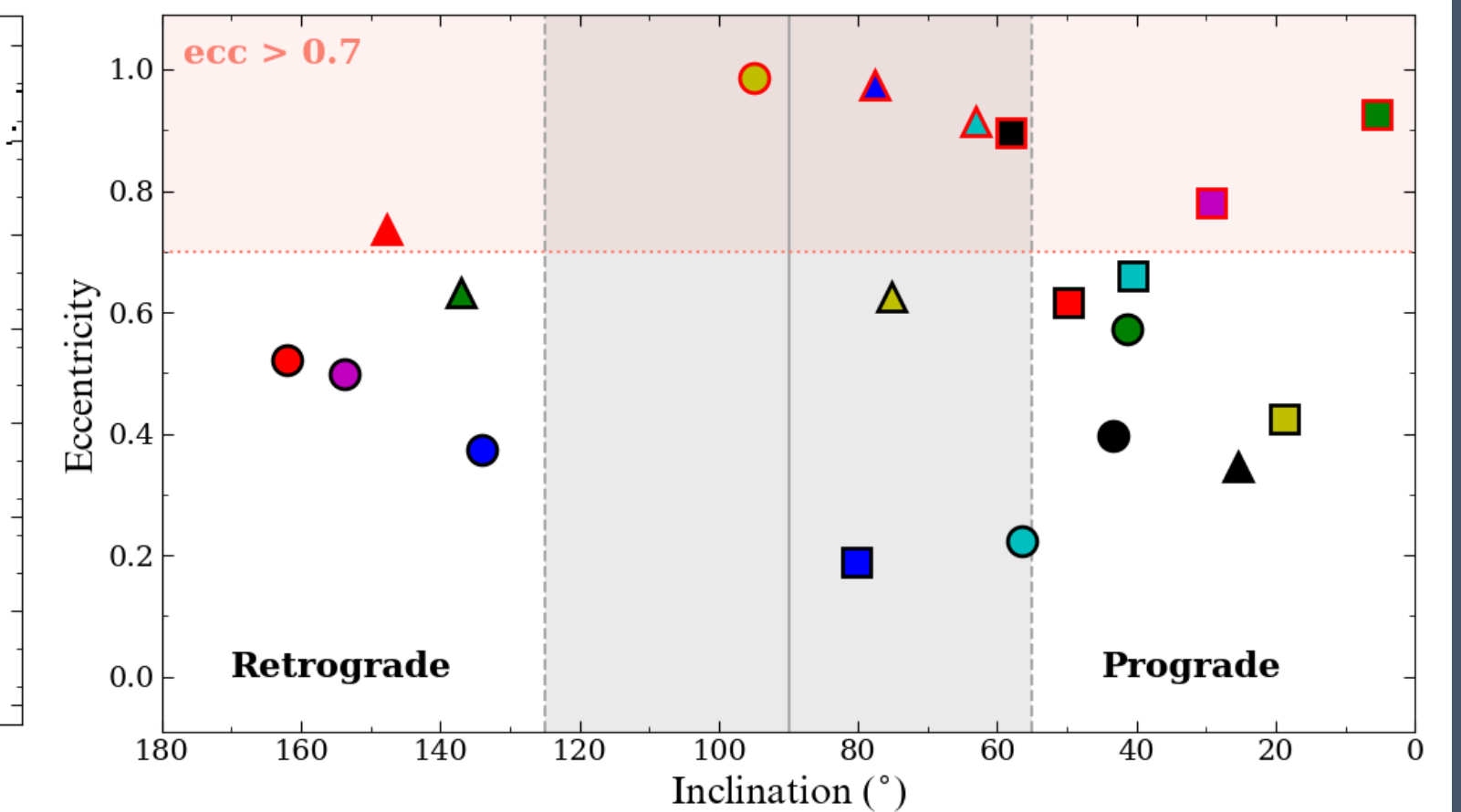
**Abstract** Extremely metal-poor (EMP;  $[\text{Fe}/\text{H}] < -3.0$ ) stars are thought to be genuine second-generation of stars because they were born from relatively pristine gas chemically enriched by one or two supernova. So, the EMP stars are important tracers for the early chemical evolution and assembly history of the Milky Way (MW). In line with this, we analyze the chemical abundance ratios derived from high-resolution spectra of about 20 EMP stars, which were obtained with Gemini/GRACES, to study the chemical evolution of the early MW by characterizing their possible progenitors. In addition, we investigate distinct kinematic signatures of the observed EMP stars to traces the assembly history of the MW by identifying their origin through the chemodynamical analysis.

## Results

We computed orbital parameters by adopting the Stäckel type potential to select stars that are dynamically associated with metal-poor stars to the substructures of MW. We adopted the radial velocities high-resolution spectra and astrometric information from Gaia EDR3 to calculate their space velocity and orbital parameters. In the case of stars with a relative parallax error of less than  $\leq 25\%$ , the parallax distance was used, and for the rest of stars ( $> 25\%$ ), the photometric distance was employed.



▲ **Figure 2.** Dynamical properties of our program stars, color-coded with their substructures. The white-black scaled map is the number density of dwarfs stars from LAMOST DR5.



▲ **Figure 3.** The distribution of our stars in the eccentricity-inclination plane. The stars with the inclination smaller than  $90^\circ$  show the prograde motion, while larger than  $90^\circ$  for the retrograde motion. Stars with high- $i$  are located in gray shaded regions. And pink shaded region represents promising GSE stars with  $e > 0.7$ .

Figure 2 and 3 show the  $E - L_z$  and eccentricity-inclination diagrams of our stars.

In Figure 3, there are seven stars with significant radial motion ( $e > 0.7$ ) typical characteristic of Gaia Sausage-Enceladus (GSE), and these are depicted throughout this poster as red edge stars. Also, GSE stars are divided into two groups: stars with low inclination orbits, those with retrograde motion, and stars with prograde motion.

## Conclusions and Summary

- We used MOOG (Snedden 1973) to estimate chemical abundance for each star. Li and Ba were estimated through a spectral fitting, while the abundance of the remaining elements was determined based on EW estimates. Due to the obstacle of the bluer wavelength of the GRACES instrument, converted C and N are estimated from low-resolution spectra. We compared the measured abundances of targets with metal-poor stars from various literatures as shown Figure 4 and 6 (see the reference in caption of each figure).
- Li was detected in more than half of our stars. Due to evolutionary effects, RGB and SGB stars have low Li because they have been diluted in the outer layer by 1st dredge-up. Since the convection zones of MSTO ( $T_{\text{eff}} > 5900 \text{ K}$ ) stars were not very deep, the initial Li would have been preserved without being destroyed. Therefore, all stars except J0102 are relatively large  $A(\text{Li}) \geq 2.0$ , but J0102 is inherently considered to have low Li.
- As shown in Figure 5, there are 8 CEMP ( $[\text{C}/\text{Fe}] > +0.7$ ) candidates, J0908 with Ba measured is CEMP-no candidates. There are also four N-rich ( $[\text{N}/\text{Fe}] > +0.5$ ) stars.
- In Figure 6, the scatter of odd-Z (Na, K, Sc) and even-Z (Mg, Ca, Ti) abundances of our stars is slightly large, but it is similar to the general trend of literature stars. The large scattering shown in Figure 6 at low metallicity indicates that our metal-poor stars were born in an environment where gas clouds were not homogeneously mixed. Of note, there are two Mg-poor stars considered members of the GSE that require further investigation. For Ti, stars with  $[\text{Fe}/\text{H}] > -3.0$  have a slightly higher Ti abundance than literature stars. Considering the low metallicity of our stars, Fe-peak (Cr, Mn, Ni, Zn) elements are thought to be mainly synthesized by CCSN rather than Type Ia SN. The only n-capture elements in the sample stars was Ba, which was measured in 10 stars, all of which are  $[\text{Ba}/\text{Fe}] < 0.0$ . Since the rest of the stars could not detect Ba feature, their Ba is also expected to be  $[\text{Ba}/\text{Fe}] < 0.0$ . Interestingly, there was no difference in overall elemental abundance between dynamically defined GSE and non-GSE stars.
- GSE stars with low orbital inclination are divided in two directions of rotation, and it might be the results of accretion events from other dwarf galaxies with low inclination prograde and retrograde orbits due to different dynamic friction, as Kim et al. 2021 suggest. However, the number of stars having different direction motions is small to constrain the difference in their chemical characteristics. It is expected that the solution to this problem will help by increasing the sample volume in 2021B, which has been analyzed in advance for some elements, and 2022B, which is scheduled to be observed. Taking into account the low metallicity of our stars together, non-GSE stars might be born in relatively low mass dwarf galaxies and disrupted to be accreted into the Galactic halo. The variety of orbital inclinations and eccentricities support this idea.

## References

- Aoki, W., Beers, T. C., Lee, Y. S., et al. 2013, *AJ*, 145, 13
- Cui, X. Q., Zhao, Y. H., Chu, Y. Q., et al. 2012, *RAA*, 12, 1197
- Demarque, P., Woo, J.-H., Kim, Y.-C., et al. 2004, *ApJS*, 155, 667
- Gaia Collaboration, Brown, A. G. A., Vallenari, A., et al. 2021, *A&A*, 649
- Kielty, C. L., Venn, K. A., Sestito, F., et al. 2021, *MNRAS*, 506, 1438
- Kim, Y. C., Demarque, P., Yi, S. K., et al. 2002, *ApJS*, 143, 499
- Kim, Y. K., Lee, Y. S., Beers, T. C., et al. 2021, *ApJL*, 911, L21
- Lee, Y. S., Beers, T. C., Sivarani, T., et al. 2008a, *AJ*, 136, 2022
- Roederer, I. U., Preston, G. W., Thompson, I. B., et al. 2014, *AJ*, 147, 136
- Spergel, D. N., Bean, R., Doré, O., et al. 2007, *ApJS*, 170, 377
- Snedden, C. A. 1973, Ph.D. Thesis
- Venn, K. A., Irwin, M., Shetrone, M. D., et al. 2004, *AJ*, 128, 1177
- Yong, D., Norris, J. E., Bessell, M. S., et al. 2013, *ApJ*, 762, 26
- York, D. G., Adelman, J., Anderson, J. E., Jr., et al. 2000, *AJ*, 120, 1579